Materials Research Proceedings **26** (2023) 319-324 https://doi.org/10.21741/9781644902431-52

Sequential linear analysis of no-tension masonry structures

Grigor Angjeliu [a *], Matteo Bruggi [b] and Alberto Taliercio [c]

Department of Civil and Environmental Engineering, Politecnico di Milano
Piazza Leonardo da Vinci, 32, 20133, Milan, Italy

[a]grigor.angjeliu@polimi.it, [b]matteo.bruggi@polimi.it, [c]alberto.taliercio@polimi.it

Keywords: Masonry, Elastic No-Tension Material, Sequential Linear Analysis

Abstract. A new application of the elastic no-tension material model is developed through Sequential Linear Analysis (SLA) to analyze masonry structures. The approach has been demonstrated to be more robust compared to incremental analysis procedures. In the SLA framework, the equilibrium state of a masonry-like material is sought through a series of linear elastic analyses. In the loading process, cracking strains are simulated by sequential reduction of the directional stiffness upon violation of the no-tension constraint in terms of principal stresses. Some applications are presented to show the effectiveness of the proposed method in analyzing masonry structures under the effect of gravity, lateral loading, and ground settlements.

Introduction

In the last decades a number of refined models have been developed for masonry structures based on the theory of plasticity and damage mechanics [1]. Although they have been shown to be quite accurate in simulating the mechanical behavior of masonry specimens and small-scale buildings tested in the laboratory, these models require many input parameters, which are hardy available in practical situations. A comparison between limit analysis solutions and finite element methods in the stability assessment of masonry structures was addressed in [2]. An alternative is the so-called no-tension material model, which completely neglects the limited tensile strength of masonry [3][4]. The reduced number of parameters required by the no-tension model makes it very appealing for unreinforced masonry constructions, compared to more refined constitutive models.

Despite the apparent simplicity of the linear elastic no tension (ENT) model, numerical issues arise as discontinuities in the stress and displacement fields have to be dealt with, leading to convergence issues. In fact, the application of ENT material models remains still limited. Readers may refer in particular to Angelillo [5], who proposed a finite element solution based on a complementary energy theorem for ENT bodies, or to Bruggi and Taliercio [6], who reformulated the analysis of no-tension structures as an energy-based problem introducing an equivalent orthotropic material.

In this contribution, the analysis of no-tension structures in plane stress conditions is dealt with through the application of a procedure of Sequential Linear Analysis (SLA). This technique provides a robust alternative to traditional incremental-iterative methods for finite element simulations, since it transforms the problem into a series of linear elastic analyses, see in particular [7]. The implementation presented here is developed through the combined application of a user subroutine in Abaqus, Python and Matlab scripts.

Two benchmark cases have been analyzed to assess the capabilities of the proposed model under vertical loads, lateral loads, and ground settlements.

Governing equations

According to [3][8], a no-tension masonry-like material has to fulfill a prescribed set of conditions. The stress tensor must be negative semidefinite:

$$\sigma_{ij} \in Sym^{-}, \tag{1}$$

Materials Research Proceedings **26** (2023) 319-324 https://doi.org/10.21741/9781644902431-52

where Sym^- is the closed cone of negative semi-definite symmetric second-order tensors.

The strain tensor is assumed to consist of two parts, an elastic part ε_{ij}^e and a latent part ε_{ij}^c accounting for cracking:

$$\varepsilon_{ij} = \varepsilon_{ij}^e + \varepsilon_{ij}^c. \tag{2}$$

Finally, the elastic strain is related to the stress σ_{ij} through the elasticity tensor C_{ijhk}, while the latent strain, ε_{ij}^c, follows the normality condition:

$$\sigma_{ij}\varepsilon_{ij}^c = 0 \quad \text{and} \quad \varepsilon_{ij}^c \in Sym^+, \tag{3}$$

where Sym^+ is the closed cone of the positive semi-definite symmetric second order tensors.

Sequential Linear Analysis Methodology

The domain occupied by the structure is discretized by 4-node plane-stress finite elements with one integration point (Fig. 1a). The SLA consists in a series of elastic analyses with modified stiffness and orientation of each element, until a stable value of the total strain energy is reached. This criterion is used as convergence condition for the iterative procedure.

Upon violation of the condition that states that all the principal stresses must be negative, the original isotropic material is replaced by an equivalent orthotropic one, with vanishing stiffness in tension. The symmetry axes, $\tilde{z}_1$, and $\tilde{z}_2$, of the equivalent orthotropic material and the principal stress directions, z_I and z_{II}, of the no-tension medium share the same orientation with respect to the general reference system Oz_1z_2 (Fig. 1b). This is achieved through a process of alignment of the symmetry axes of the equivalent orthotropic material with the principal stress directions, z_α, $\alpha = I, II$, detected in the no-tension medium.

The principal stresses are computed as the eigenvalues of the stress tensor at the Gauss points, whereas the principal directions are found as the relevant eigenvectors.

In order to track cracking strains, at each Gauss point, two nondimensional material densities $\rho_i \in (0,1]$ are introduced along the material axes; these parameters govern the stiffness penalization of the orthotropic material along $\tilde{z}_1$ and $\tilde{z}_2$. The material density ρ_i is related to the damage variable D_i through the expression $D_i = (1 - \rho_i)$. If any of the principal stresses becomes positive, the material density variable is initialized with a value, $\rho_0 = 0.25$, whereas further reductions are performed using a quadratic reduction factor, i.e.:

$$\rho_{k+1,i} = 1 - \left(1 - \rho_{k,i}\right)^2, i = 1,2. \tag{4}$$

In each material direction, the model can capture elastic (negative) compressive strains, or positive strains, which correspond to cracking strains. In the latter case, a scaled stiffness is computed in the direction where the principal stress becomes positive, to account for cracking.

The stress-strain law written in matrix form in the general reference system reads:

$$\boldsymbol{\sigma} = \boldsymbol{D}\,\boldsymbol{\varepsilon} \tag{5}$$

where:

$$\boldsymbol{D} = \boldsymbol{T}(\theta)\ \ \widetilde{\boldsymbol{D}}\ \ \boldsymbol{T}(\theta)^T \tag{6}$$

being T a transformation matrix and θ the angle between z_1 and $\boldsymbol{z_I}$. In plane stress, the stiffness matrix in the material (principal stress) reference system reads:

$$\widetilde{\boldsymbol{D}} = \frac{1}{1-\tilde{\nu}_{12}\tilde{\nu}_{21}}\begin{bmatrix} \tilde{E}_1 & \tilde{\nu}_{12}\tilde{E}_2 & 0 \\ \tilde{\nu}_{21}\tilde{E}_1 & \tilde{E}_2 & 0 \\ 0 & 0 & \tilde{G}_{12}(1-\tilde{\nu}_{12}\tilde{\nu}_{21}) \end{bmatrix} \tag{7}$$

Materials Research Proceedings **26** (2023) 319-324 https://doi.org/10.21741/9781644902431-52

being $\tilde{E}_1$ and $\tilde{E}_2$ the elastic moduli of the equivalent orthotropic material along the axis $\tilde{z}_1$ and $\tilde{z}_2$, respectively, $\tilde{G}_{12}$ the in-plane shear modulus, and $\tilde{\nu}_{12}$ $\tilde{\nu}_{21}$ the material Poisson's ratios such that $\tilde{\nu}_{21}\tilde{E}_1 = \tilde{\nu}_{12}\tilde{E}_2$. When the negative stress criterion is violated at any Gauss point, the equivalent moduli are reduced with respect to those of the original material as follows:

$$\tilde{E}_1 = \rho_1 E_0, \quad \tilde{E}_2 = \rho_2 E_0, \quad \tilde{G}_{12} = \rho_1\rho_2 \frac{E_0}{2(1+\nu)} \tag{8}$$

being E_0 and ν the elastic constants of the original isotropic material. At the same time, the Poisson's ratios of the equivalent orthotropic material are given by:

$$\tilde{\nu}_{12} = \rho_2\nu, \quad \tilde{\nu}_{21} = \rho_1\nu. \tag{9}$$

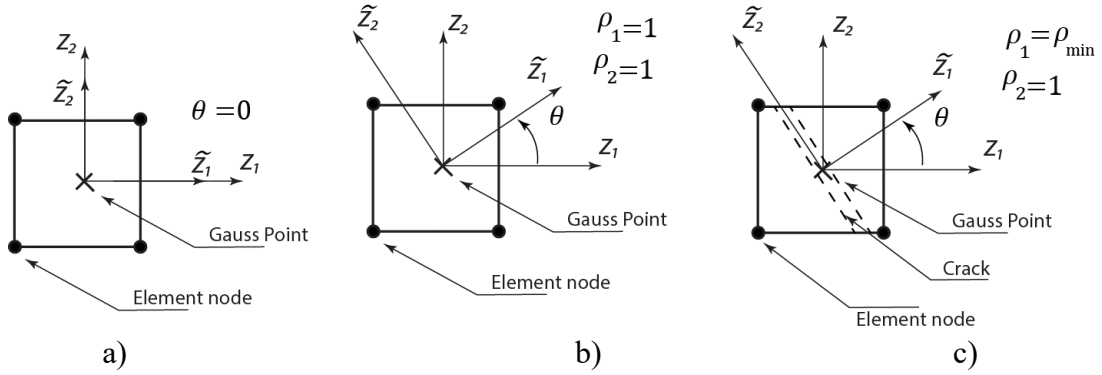

Fig. 1. State of stress in a plane element: a) initial state, b) alignement of the material axes with the principal stress directions, c) damage onset normal to a nonnegative principal stress.

Applications no. 1: Masonry panel under gravity loads and soil settlements

The aim is to test the ability of the ENT model to simulate the behavior of a masonry wall over a strip foundation subjected to ground settlements along a portion of its constrained boundary. The wall is supposed to be 3.2 m long, 0.6 m high and 0.1 m thick; only the central part, for an extension of 1.2 m, is affected by settlements (Fig. 2). The initial modulus of elasticity, E_0, is assumed to be equal to 1020 MPa. The panel is discretized with a mesh 75 x 75 mm^2. The wall is analyzed under self-weight condition, while settlements are simulated by removing all the constraints at the nodes of the central region.

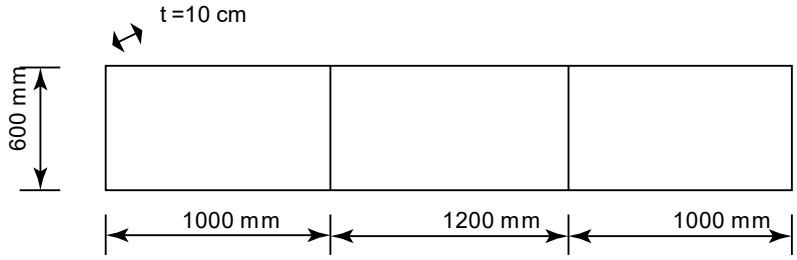

Fig. 2. Scheme of a masonry wall experiencing ground settlements in the central region.

The numerical simulations show the formation of a relieving arch (Fig. 3), which is typical of no-tension bodies. Starting from the ends of the fixed boundary, the direction of the principal compressive stress decreases and becomes horizontal at the middle of the unconstrained region. The rest of the model is not affected by settlements, and only nearly vertical compressive stresses are found.

The formation of the arch-like compressive stress path affects the displacement field significantly. In fact, compared to the conventional elastic case (Fig. 4a), where settlements affect

Materials Research Proceedings **26** (2023) 319-324 https://doi.org/10.21741/9781644902431-52

also the neighboring regions, in the case of the ENT material displacements of non-negligible amplitude arise only beneath the inner arch (Fig. 4b). The zone above experiences much smaller displacements, whereas the rest of the model is virtually undeformed. This is in line with the schemes proposed by Mastrodicasa [9] regarding the effects of settlements in masonry walls.

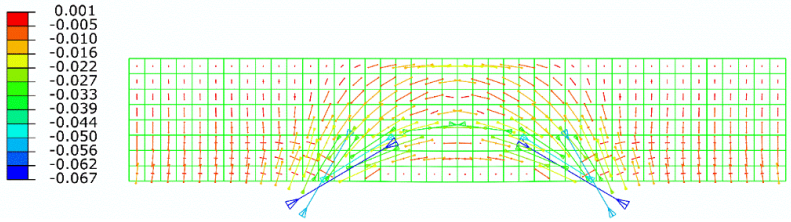

Fig. 3. Wall with settlements. Principal stresses from the ENT simulation.

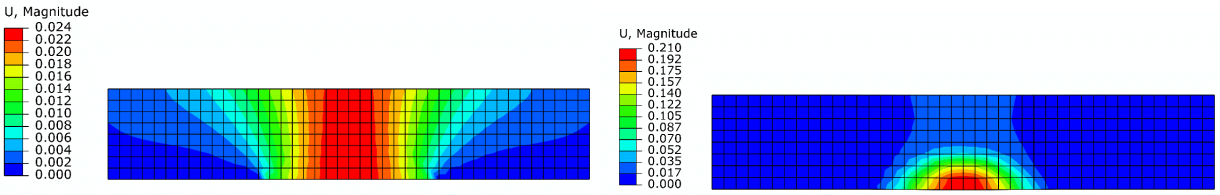

Fig. 4. Wall with settlements. Displacement contour plots: a) elastic model with symmetric behaviour in tension/compression, b) Elastic No-Tension model.

Application no. 2: Masonry panel under vertical pressure and horizontal loading

A slender masonry panel with dimensions 2.7m x 1.1m x 0.102m was tested at TU Delft [10] (experiment TUDCOMP-20): this experiment will be now adopted to validate the proposed numerical procedure. The top of the panel is loaded with a uniform vertical pressure of 0.63MPa. The pressure is applied through a horizontal steel beam and is kept constant during the experiment.

The domain is discretized by 100 mm x 100 mm square elements. The top steel beam is modelled though a row of elastic elements in the mesh, and is allowed to rotate similarly to the experimental setup. The material properties are: E_0=4972 MPa, ν=0.16. The compressive strength of the material, f_c, reported by the experimenters, is of 6.35 MPa.

In Fig. 5 the distribution of the principal stresses and that of the "void" phase (elements with biaxial damage, in blue) are both shown at the first converged stage in which any of the principal compressive stresses reaches the strength limit f_c.

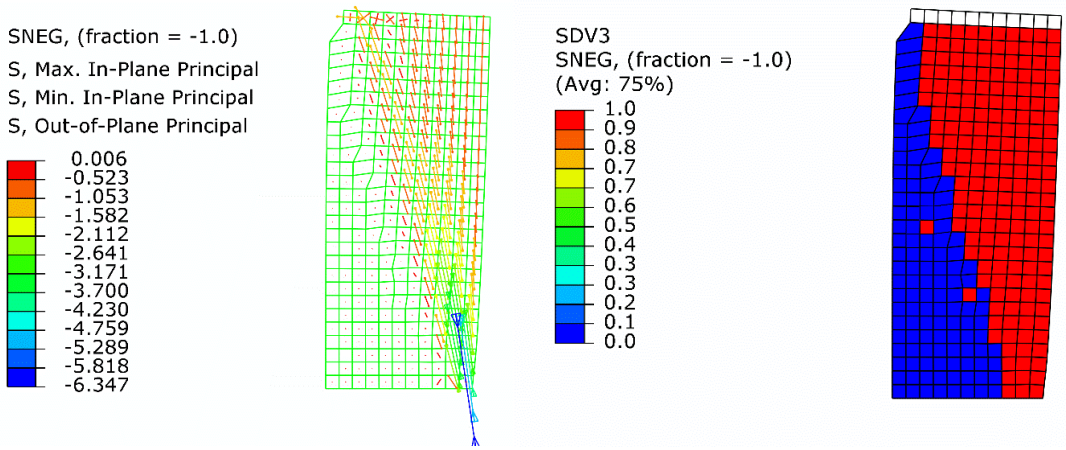

Fig. 5. Panel under horizontal loading, first SLA stage in which f_c is reached in some element: a) distribution of the principal stresses in the masonry wall, b) distribution of "void" elements, i.e. those with biaxial damage (in blue).

The collapse load is estimated in 12.77 kN. This value matches quite well the horizontal branch of the experimental curve whose maximum value is 12.8 kN.

The analytical calculation considering a simple panel overturning under vertical and horizontal loads gives a value of 14.4 kN, if the hinge is formed at the corner, or a value of 13.1 kN, if the hinge is considered 50 mm far away. The second value seems to be more representative of the considered case, since in the numerical model the hinge is allowed to occur at the midpoint of the side of a finite element, that is, at 50mm from the corner. Therefore, the difference between the numerical failure load and the analytical model is about 2.4%.

Regarding the displacement capacity, it must be remarked that limit analysis can predict only the limit load. However, if we consider a finite strength in compression, the predicted displacements when f_c is reached is 13.2 mm. Additional converged steps were obtained, but the compressive strength of masonry is exceeded.

Conclusions

In this contribution, the ENT model has been implemented in the framework of sequential linear analysis, which consists in a number of elastic analyses sequentially launched. The properties of the equivalent orthotropic material that replaces the ENT material to avoid the occurrence of tensile stresses are obtained through a penalization procedure.

The proposed approach was used to analyze masonry structures subjected to prescribed loads or ground settlements. In the latter case, the cracking strains computed by the SLA procedure match the real crack pattern expected at incipient collapse fairly well. Also, the limit load of a panel tested under increasing horizontal load and dead vertical load was predicted with good accuracy.

An advantage of the proposed approach compared to traditional incremental approaches is its inherent robustness.

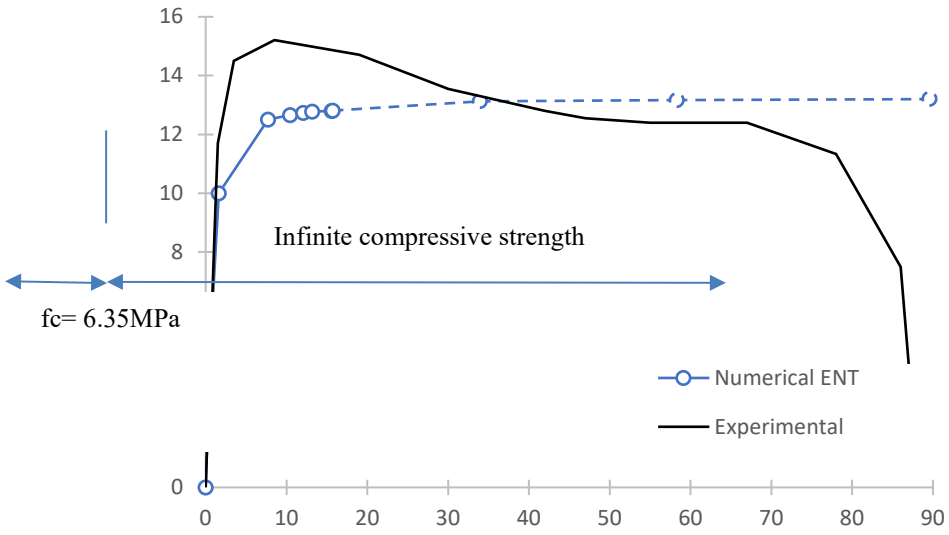

Fig. 6. Panel under horizontal loading. Comparison of experimental and numerical shear vs displacement capacity curve. Displacement are in mm, loads in kN.

References

[1] P.B. Lourenço, J.G. Rots, J. Blaauwendraad, Continuum Model for Masonry: Parameter Estimation and Validation, Journal of Structural Engineering, 124 (1998) 642-652. https://doi.org/10.1061/(ASCE)0733-9445(1998)124:6(642)

[2] C. Cusano, G. Angjeliu, A. Montanino, G. Zuccaro, C. Cennamo, Considerations about the static response of masonry domes: a comparison between limit analysis and finite element method, International Journal of Masonry Research and Innovation, 6 (2021) 502-528. https://doi.org/10.1504/IJMRI.2021.118835

[3] E. Sacco, Modellazione e calcolo di strutture in materiale non resistente a trazione, Rend. Mat. Acc. Lincei, 1 (1990) 235-258. https://doi.org/10.1007/BF03001757

[4] M. Angelillo, Constitutive relations for no-tension materials, Meccanica, 28 (1993) 195-202. https://doi.org/10.1007/BF00989121

[5] M. Angelillo, L. Cardamone, A. Fortunato, A numerical model for masonry-like structures, Journal of Mechanics of Materials and Structures, Volume 5, No. 4 (2010). https://doi.org/10.2140/jomms.2010.5.583

[6] M. Bruggi, A. Taliercio, Analysis of no-tension structures under monotonic loading through an energy-based method, Computers & Structures, 159 (2015) 14-25. https://doi.org/10.1016/j.compstruc.2015.07.002

[7] M. Pari, M. Hendriks, J.G. Rots, Non-proportional loading in sequentially linear solution procedures for quasi-brittle fracture: A comparison and perspective on the mechanism of stress redistribution, Engineering Fracture Mechanics, 230 (2020) 106960. https://doi.org/10.1016/j.engfracmech.2020.106960

[8] G. Del Piero, Constitutive equation and compatibility of the external loads for linear elastic masonry-like materials, Meccanica, 24 (1989) 150-162. https://doi.org/10.1007/BF01559418

[9] S. Mastrodicasa, Dissesti statici delle strutture edilizie. Diagnosi e consolidamento, (1958).

[10] R. Esposito, G.J.P. Ravenshorst, Quasi-static cyclic in-plane tests on masonry components, Report C31B67WP3-4, Delft University of Technology, 2017.